Journal of Marine Research, 44, 203–225, 1986

A model for the vertical flux of nitrogen in the upper ocean: Simulating the alteration of isotopic ratios

by Mark A. Altabet[1,2] Allan R. Robinson[3] and Leonard J. Walstad[3]

ABSTRACT

An idealized, one-dimensional, constant diffusivity mathematical model for the study of the vertical flux of nitrogen in the upper-ocean is presented. We attempt to simulate observed patterns in vertical profiles for the natural abundance of ^{15}N in particulate organic nitrogen (PON) and the concentrations of PON and NO_3^-. The concentration of phytoplankton nitrogen (II) increased as a result of either increasing the upward flux of NO_3^- (N) or by increasing the residence time of II. A minimum in the $\delta^{15}N$ of phytoplankton nitrogen (δ_2) appeared near a maximum in II at the inflection point of the N profile. Increasing the residence time or the vertical eddy diffusivity, reduced the amplitude of the δ_2 profile. The model was able to produce reasonably good simulations of observed profiles from two warm-core rings, Rings 82-E and 82-H, using the most appropriate values for the light extinction coefficient and the residence time of PON. These results lend general support to current views regarding the nature and significance of the vertical fluxes of nitrogen in the upper-ocean and hypotheses presented previously concerning the factors which affect the $\delta^{15}N$ of PON.

1. Introduction

The vertical fluxes of nitrogen in the open ocean are important components of the biological and chemical cycles of the marine environment. Nitrogen is removed from the euphotic zone principally via the downward flux of particulate matter in the form of relatively large, fast sinking particles. The upward flux of NO_3^- into the euphotic zone is the primary source of "new" nitrogen and on average must balance the downward flux of particulate nitrogen (Eppley and Peterson, 1979; Eppley *et al.,* 1983). The magnitude of the downward particle flux has been related to the magnitude of primary productivity (Suess, 1980; Deuser and Ross, 1980; Betzer *et al.,* 1984; Bishop and Marra, 1984). However, the processes which link the upward flux of NO_3^- to the downward flux of particles remain poorly understood.

Altabet and McCarthy (1985) hypothesized that vertical variations in the natural

1. Museum of Comparative Zoology, Harvard University, Cambridge, Massachusetts, 02138, U.S.A.
2. Present address: Woods Hole Oceanographic Institution, Woods Hole, Massachusetts, 02543, U.S.A.
3. Center for Earth and Planetary Physics, Harvard University, Cambridge, Massachusetts, 02538, U.S.A.

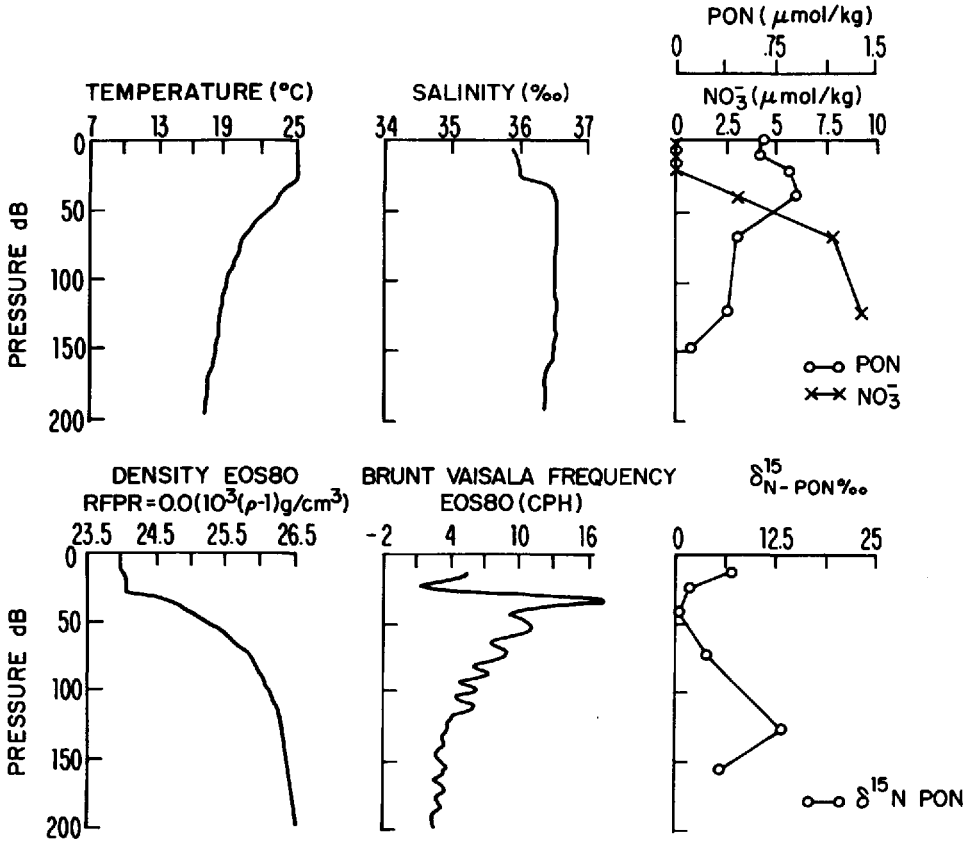

Figure 1. Representative profile for NO_3^- concentration, PON concentration, $\delta^{15}N$ of PON, temperature, salinity, density, and Brunt Väisälä frequency from Ring 82-E.

abundance of ^{15}N in particulate organic nitrogen (PON) will occur in response to the fluxes of nitrogen into and out of the euphotic zone. The "δ" convention is used as a relative measure of the ratio of ^{15}N to ^{14}N:

$$\delta^{15}N = \left[\frac{^{15}N/^{14}N \text{ sample}}{^{15}N/^{14}N \text{ standard}} - 1\right] \times 1000.$$

The units are "per mil" (‰). The standard is usually atmospheric N_2 which is considered to have a globally constant $^{15}N/^{14}N$ ratio (Mariotti, 1983).

Altabet and McCarthy (1986) present vertical profiles for the concentration of NO_3^-, the concentration of particulate organic nitrogen (PON), and the $\delta^{15}N$ of PON from the upper 200 m of 4 warm-core rings and the Sargasso Sea during oligotrophic, stratified conditions (see Fig. 1 for a representative profile). It was demonstrated that a minimum of the $\delta^{15}N$ of PON often occurs together with the top of the nitracline and a

maximum in PON. The top of the nitracline is the depth interval below the depth at which NO_3^- becomes detectable where the NO_3^- gradient is usually largest with depth. The top of the nitracline also corresponded to the depth of the euphotic zone. It was surmized that these persistent vertical patterns in NO_3^-, PON concentration and the $\delta^{15}N$ of PON result from the combined effect of the localization of NO_3^- uptake to the region at the top of the nitracline and the fractionation of nitrogen isotopes in the uptake of NO_3^- by phytoplankton. In addition, the observed increase in the $\delta^{15}N$ of PON below the top of the nitracline was concluded to be the result of isotopic fractionation in the process of PON degradation. In the present work, a model is developed to simulate, mathematically, the observed vertical patterns for the $\delta^{15}N$ of PON as a test of these hypotheses.

Many investigators have constructed models to simulate the vertical distribution of biological and chemical properties in the upper water column. Most have concentrated on chlorophyll as the quantity of interest. This is in part due to the observation of a subsurface chlorophyll maximum near the base of the euphotic zone as a ubiquitous feature of the oligotrophic ocean (Anderson, 1969; Venrick *et al.*, 1973; Cullen and Eppley, 1981 as examples). A few of these models have included nitrogen fluxes as important terms in their models (Jamart *et al.*, 1977; Kiefer and Kremer, 1981). The Kiefer and Kremer model, however, did not permit any vertical exchange between levels of the model. Cline and Kaplan (1975), in their investigation of denitrification, produced a model simulating the vertical profile for the $\delta^{15}N$ of NO_3^- in the low O_2 region of the Eastern Tropical Pacific.

The current model represents a synthesis and extension of both the Jamart model and the Cline and Kaplan model in the sense that the effect of upper-ocean processes on nitrogen isotope abundances is explored. The model confines itself to simulating the vertical distributions of four qualtities: NO_3^- (N), the $\delta^{15}N$ of NO_3^- (δ_1), phytoplankton nitrogen (II), and the $\delta^{15}N$ of phytoplankton nitrogen (δ_2). A schematic of the processes to be considered is found in Figure 2a. Nitrogen and ^{15}N is transferred between the N and II boxes by the processes of phytoplankton NO_3^- uptake and the decay of phytoplankton nitrogen back to NO_3^-. Nitrogen is lost from the system by the downward flux of particulate nitrogen. Transfer between levels occurs via turbulent mixing. Horizontal processes are excluded from the model formulation. All model solutions fit a general pattern with certain critical features (Fig. 2b). A complete list of the model variables and parameters is presented in Table 1.

It need be stressed that the model has been kept as simple as possible, especially with regard to physical processes, in order to understand the fundamental interaction of biological processes and to evaluate the dependencies of critical parameters. As a result, a qualitative comparison between the model results and data will be stressed. Consideration of nitrogen isotopes serves to constrain the modelled nitrogen fluxes providing an additional test of the general validity of the model. This study is a first step leading to the development of more sophisticated models and in the closing section,

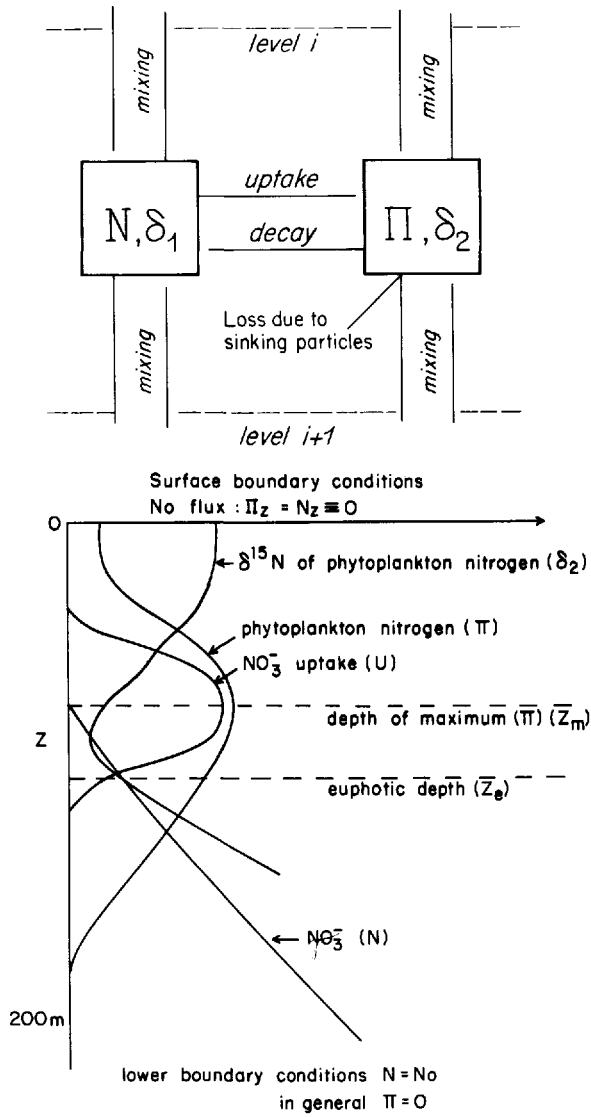

Figure 2. (A) Schematic representation of the processes included in the formulation of the model presented. (B) A typical model solution simulating the co-occurrence of a maximum in phytoplankton nitrogen (Π) with a minimum in $\delta^{15}N$ (δ_2) at the top of the nitracline. The depth of the euphotic zone (z_e) is a model parameter and is discussed in the "Model equations" section. The depth of Π maximum (z_m) is a model result and will be discussed in the "Results" section.

Table 1. Variable and parameter list.

Variables:

N	μmol/kg	NO_3^- concentration
Π	μmol/kg	Phytoplankton nitrogen concentration
δ_1	‰	$\delta^{15}N$ of NO_3^-
δ_2	‰	$\delta^{15}N$ of Π
U	μmol/kg-day	NO_3^- uptake rate
V_m	μmol/kg-day	Maximal light dependent NO_3^- uptake rate
z	meters	Depth

Parameters:

K	5 to 100 m^2/day	Vertical eddy diffusivity
F	0.5 to 0.01 day^{-1}	Particle flux coefficient
D	0.1 to 0.01 day^{-1}	Π decay coefficient
S	0.01 to 1.0 μmol/kg	Half saturation constant for NO_3^- uptake
L	0.05 to 0.16 $meter^{-1}$	Light extinction coefficient
M	100 to 1 (nondimensional)	Photosynthetic response coefficient
μ_m	1 to 2 day^{-1}	Maximal growth rate
N_0	6.3 to 63 μmol/kg	NO_3^- concentration at $z = 200$ meters
$\delta_1(N_0)$	5‰	$\delta^{15}N$ of NO_3^- at $z = 200$ meters
B_1	5 to 15‰	Fractionation coefficient for NO_3^- uptake
B_2	5 to 15‰	Fractionation coefficent for Π decay

Derived quantities

$\int U$	Integrated NO_3^- from $z = 0$ to $z = 200$
$\int \Pi$	Integrated Π from $z = 0$ to $z = 200$
$\int D$	Integrated decay from $z = 0$ to $z = 200$
z_m	Depth of maximum in U

a more rigorous comparison with data is made to assess the model deficiencies which may be corrected in future studies.

2. The model equations

The equations describing the time dependent changes in Π and N are as follows (differentiation is with respect to the subscripted variables):

$$N_t = K \cdot N_{zz} - U + D \cdot \Pi \tag{1}$$

$$\Pi_t = K \cdot \Pi_{zz} + U - D \cdot \Pi - F \cdot \Pi. \tag{2}$$

Note that z is positive downward.

The first terms on the right-hand side in Eqs. 1 and 2 are the turbulent flux terms. K is the vertical eddy diffusivity. These terms are parameterizations of the Reynold's vertical turbulent flux terms: $(\overline{\Pi' W'})_z$ and $(\overline{N' W'})_z$. Other than a Ring 82-E example in which we apply a variable K, only a constant eddy diffusivity will be considered in this paper. Therefore the vertical mixing is formulated as in Eq. 1 rather than as $(K \cdot N_z)_z$. Experiments involving variable K and a bulk mixed layer indicate that qualitatively the profiles do not change if z_m, the depth of maximum in Π, is deeper than the mixed layer. The second term, U, is the uptake of N into Π and will be discussed in further detail below.

The third term on the right-hand side of Eqs. 1 and 2 describes as a first order process, the decay of Π back into N with D as the decay constant. The parameter D is depth dependent:

$$\text{If } z < z_e; \qquad D = 0$$

$$\text{If } z > z_e; \qquad D = \text{Constant}$$

where z_e is the euphotic depth, below which Π begins to degrade back to N. Π is degraded into dissolved forms of nitrogen such as NH_4^+ and urea both above and below z_e. Above z_e these forms of dissolved nitrogen are immediately reassimilated by phytoplankton. Only below z_e does nitrification to N occur and the complete process from Π to N is modelled by the term $D \cdot \Pi$. In practice, z_e is set (and kept constant) for each model run. More than 90% of N uptake occurs above this level in every case.

The last term on the right-hand side in Eq. 2 expresses the loss of Π from the system via the downward particle flux. It has been concluded that the primary loss of particulate matter (and thus nitrogen) from the euphotic zone is in the form of large, fast sinking particles; ca. 100 m/day (Bishop *et al.*, 1977; Lorenzen and Welschmeyer, 1983). The term $F \cdot \Pi$ is equal to the rate of formation of these large particles which are assumed to be immediately lost from the system.

The process of large particle formation is thought to be due to a variety of phenomenon including the production of zooplankton fecal pellets (Honjo and Roman, 1978) and the accretion of small particles into "marine snow" (Shanks and Trent, 1979). However, no theoretically or empirically derived relationship has been established between the concentration or quality of particles in the euphotic zone and the downward particle flux. As a result, a first order dependence was used as the simplest expression that would allow for the simulation of the observed verticle profiles. The parameter F in this formulation, however, is of particular interest in that when $F \cdot \Pi$ is the primary loss term for Π, $1/F$ is the residence time for Π in the system. As a result, comparisons can be made with values for residence time derived from field data.

Uptake, U, is a function of Π and N, in addition to the input function $V_m(z)$:

$$U = V_m \cdot \Pi \cdot N/(N + S) \tag{3}$$

S is the half saturation constant for uptake. In Eq. 3, the maximal uptake rate, V_m, is a function of depth but not of time. $V_m(z)$ is given by the following two equations:

$$I = I_0 \cdot e^{-L \cdot z} \tag{4}$$

$$V_m = \mu_m \cdot I/(I + I_k). \tag{5}$$

Eq. 4 expresses the extinction of light, I, with depth. I_0 is the light intensity at the surface; $z = 0$. Eq. 5 describes the relationship between V_m and I as a hyperbolic function with I_k as a half saturation constant and μ_m as the maximal growth rate. This formulation ignores the possible effects of photoinhibition. For convenience, a nondimensional parameter, M, is used to replace I_0 and I_k. M, the photosynthetic response coefficient, is defined as being equal to I_0/I_k.

The equations for δ_1 and δ_2 are as follows:

$$(N \cdot \delta_1)_t = K \cdot (N \cdot \delta_1)_{zz} - U \cdot (\delta_1 - B_1) + D \cdot \Pi \cdot (\delta_2 - B_2) \tag{6}$$

$$(\Pi \cdot \delta_2)_t = K \cdot (\Pi \cdot \delta_2)_{zz} + U \cdot (\delta_1 - B_1) - F \cdot \Pi \cdot \delta_2 - D \cdot \Pi \cdot (\delta_2 - B_2). \tag{7}$$

These equations are similar to the formulation given the Cline and Kaplan model where the flux of ^{15}N is modelled by the term $N \cdot \delta$. U in their model, however, was assumed to decay exponentially with depth with no dependence on NO_3^-. See Cline and Kaplan (1975) for the approximations used in the derivation of Eqs. 6 and 7. The parameters B_1 and B_2 are related to the isotopic fractionation factors (β) for the processes of NO_3^- uptake and particle decay respectively.

$$B_1 \text{ or } B_2 = (\beta - 1) \times 1000$$

$$\beta = r_{14}/r_{15}.$$

The terms r_{14} and r_{15} are the first order rate coefficient for the transfer for ^{14}N and ^{15}N respectively. Cline and Kaplan (1975) use an expression for isotopic fractionation which is similar to the second and third terms on the right-hand side of Eqs. 6 and 7. Their formulation, though has β as a divisor. It has been dropped from the present formulation since its value does not exceed 1.015.

The boundary conditions for the model are:

$$\text{At } z = 0: \quad N_z = 0, \quad \Pi_z = 0, \quad (N \cdot \delta_1)_z = 0, \quad (\Pi \cdot \delta_2)_z = 0$$

$$\text{At } z = 200: \quad N = N_0, \quad \Pi = 0, \quad \delta_1 = \delta_1(N_0)\,.$$

Flux of all quantities through the surface is zero. There is assumed to be an infinitely large reservoir of N below 200 m, with N_0 as the concentration of N. Setting $\Pi = 0$ below 200 m could have the effect of permitting the lower boundary to be a sink for Π. In practice, Π for a large majority of the model runs goes to zero well above 200 m such that no flux through the lower boundary occurs. If Π at 200 m were set at some finite Π_0, the lower boundary would then become a source for Π into the model region via turbulent mixing and as such would not be a desired result.

The model as formulated differs from the Jamart model in a number of ways. An equation for the flux of NH_4^+ is not specified and the role of grazers in recycling nitrogen is ignored. Altabet and McCarthy (1985) concluded that the recycling of nitrogen through NH_4^+ in the euphotic zone (or urea and amino acids) would not significantly alter the $\delta^{15}N$ of PON (here considered equivalent to Π). Below the euphotic zone, the action of bacteria and microheterotrophs in degrading PON would alter the $\delta^{15}N$ of PON. This degradation and subsequent nitrification of the dissolved products has been parameterized by the decay term $D \cdot \Pi$. Only rarely were NH_4^+ concentrations above the limit of detection throughout the Warm Core Rings Program (J.J. McCarthy, unpublished data). NO_2^- concentrations were occasionally found above 0.1 μmol/kg (D. Kester, pers. comm.).

The Jamart model includes a term for the sinking of phytoplankton. It has been demonstrated that the majority of the suspended particles in the water column are of small size with very small sinking velocities (Bishop *et al.*, 1977). Size fractionation studies done as part of the Warm Core Rings Program have resulted in similar conclusions for chlorophyll (G Hitchcock, pers. comm.) and ATP (C. Langdon, pers. comm.). The Jamart model did not include a term for the rapid sinking of large particles. In fact, they have no explicit term for the loss of nitrogen from the euphotic zone. It appears that the primary loss term for nitrogen in their model is the grazing term.

The Jamart model uses a vertical eddy diffusivity (K) which varies with depth; the value is high in the depth interval corresponding to the mixed layer and decays with depth below. In the present model, K is held constant with depth. The field observations presented in Altabet and McCarthy (1986) show that, for the most part, the maximum in PON and the minimum in $\delta^{15}N$ of PON (δ_2) occur below the base of the mixed layer; at a depth of 20 to 60 m in the region at the top of the nitracline. As a result, it was assumed that it was primarily the value of K in this region that would influence the major flux terms, especially those concerning N.

a. The parameters. The values for vertical eddy diffusivity (K) were based on literature values considered typical for the seasonal thermocline, 5 to 20 m^2/day (Anderson, 1978; Eppley *et al.*, 1979; King and Devol, 1979) calculated on the basis of the observed NO_3^- profile and NO_3^- utilization in the euphotic zone. Higher values were used to test the general effects of larger mixing rates which would be expected when stratification was either weak or not present in the upper 200 m.

Measurements of the half saturation constant (S) for NO_3^- uptake by phytoplankton grown in culture has been reported (Eppley *et al.*, 1969) and are used to set the range in values tested by the model. The values used for the light extinction coefficient (L) are those which were directly measured *in situ* (C. Ventsch, pers. comm.). Eppley *et al.* (1969) present data for the relationship between light level and NO_3^- uptake which suggest that under oligotrophic conditions the value of M should be near 50. The

value of μ_m is taken from literature values (Eppley, 1972) for the maximal growth of phytoplankton in culture for temperatures between 18 and 24°C, corresponding to water temperatures found for the euphotic zone of the warm-core rings studied in the Warm Core Rings Program.

The values of D used were between 0.1 and 0. Recent investigations into the decay of sediment trap collected material suggest values between 0.01 and 0.0001 are most appropriate (Gardner *et al.*, 1983). It was found, though, that the higher values of D used were necessary to achieve realistic profiles for δ_2. The range of F is from 0.5 to 0.01, corresponding to a range in residence time of 2 to 100 days. This range is similar to the one reported by Eppley *et al.* (1983).

The value of B_1 is within the range reported for the uptake of NO_3^- by diatoms (Wada and Hattori, 1978). The range in B_2 used is the same as for B_1.

The values of N_0 were chosen to give reasonable values for the vertical NO_3^- gradient, N_z; 0.02 to 0.4 μmol kg^{-1} m^{-1}. The value for $\delta_1(N_0)$ was set at $+5.0$‰ for all model runs. The exact value of $\delta_1(N_0)$ is not critical since in the analysis of the model results, it is primarily the relative changes in $\delta^{15}N$ which are considered. This value for $\delta_1(N_0)$ is similar to measurements made by other investigators for the $\delta^{15}N$ of NO_3^- (Cline and Kaplan, 1975; Liu, 1979; Miyake and Wade, 1967). Altabet and McCarthy (1985), however, reported values for the $\delta^{15}N$ of NO_3^- from Ring 82-B between $+2.0$ and $+4.0$‰.

b. Solutions: stability and convergence. Other than the trivial solution, ($\Pi = 0$, $N = N_0$), there is no analytic steady state solution of the model equations known to us. Perturbation expansions and boundary layer methods were useful in the exploration of the dynamics but have not yielded a satisfactory approximation solution. The complexity of analytic approximation and the relative ease of numeric solutions for the system led us to choose this method of parametric investigation. Furthermore, this is the first step in the development of a time-dependent, three-dimensional, upper-ocean model including accurate upper-ocean physics and biological processes.

Numerical solutions were obtained by integrating the second order finite difference form of Eqs. 1, 2, 6 and 7 using an Euler time step. Both constant and variable grid spacing was used. In every case, the grid spacing is 2 m between 30 and 140 m depth. Integration proceeded until a steady state as defined by

$$\max\left(\frac{\partial N}{\partial t}/\max(N),\ \frac{\partial \Pi}{\partial t}/\max(\Pi)\right) \leq 10^{-5}/\text{day}$$

was achieved. The model equations indicate that time scales of 5 to 1000 days are present for typical values of the parameters. The slower time scale involves the equilibration of the N profile below the euphotic zone. The faster time scales involve N uptake and downward particle flux. Numerical results support this analysis. Typically

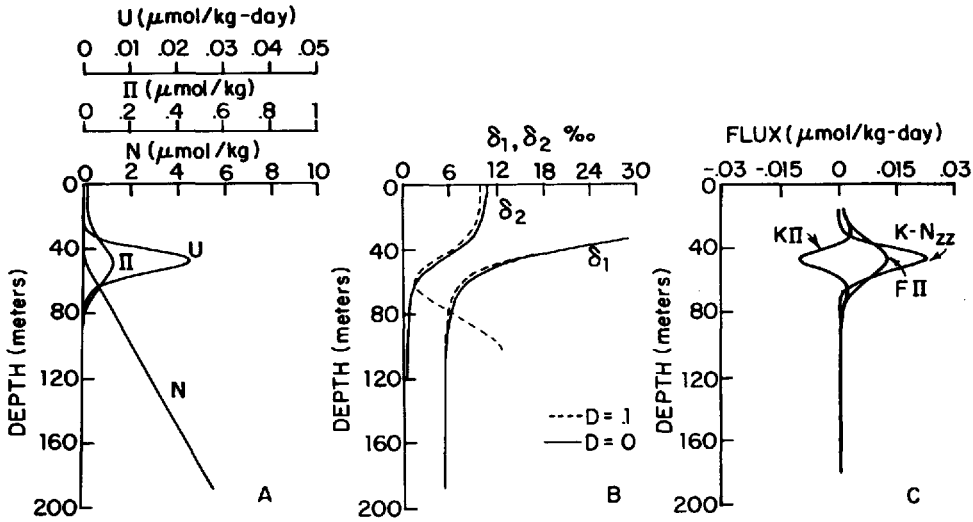

Figure 3. General solution for the model. (A) profiles for Π, N, and U. (B) profiles for δ_1 and δ_2; note comparison between profiles for $D = 0$ and $D = 0.1$. (C) profiles for the flux terms $K \cdot N_{zz}$, $K \cdot \Pi$, and $F \cdot P$. These results are those for run 6 ($D = 0$) and run 7 ($D = 0.1$).

1000 days are required to reach the rather stringent steady state requirement, however the profiles of N and Π within the euphotic zone reach steady state in 2 to 3 weeks.

Various initial conditions were used for several parameter choices. In every case, the final state was independent of the initial condition unless the initial condition includes $\Pi = 0$. This indicates that the nontrivial solutions obtained are stable. The trivial solution is unstable as may be shown by an analytical stability analysis. Convergence to steady state was smooth with the exception of an initial growth of Π above z_m due to excess N in this region. The Π which accumulates is then removed by the term $F \cdot \Pi$ in 5 to 10 days.

Further experiments with choice of time step Δt and grid spacing h indicate that our choice of $\Delta t \leq \min(h^2/2K)$ are appropriate for the parameter range explored. Based on these results we conclude that the numerical solutions obtained are stable and accurate solutions to the model equations.

3. Results

Solutions to the model were generated, varying the parameters throughout the ranges listed in Table 1. It became apparent that these solutions have several general features in common with regard to the simulated vertical profiles for N, Π, δ_1, and δ_2. Representative profiles are presented in Figures 3a and 3b (Runs 6 and 7). Table 2 lists the parameters used for these and all other model runs. Note the presence of a maximum in Π near the depth level where N approaches 0 with both δ_1 and δ_2 increasing from this depth level toward the surface. A maximum in U (Fig. 3a) occurs

Table 2. Model run table listing the variation in parameters and the primary features of the model solution.

Part A. Variations in the eddy diffusivity (K), the large particle flux coefficient (F), and the Π decay coefficient (D).

$\mu_m = 1.5$, $L = .11$, $M = 50$, $S = .1$, $N_0 = 6.3$, $B_1 = 10$, and $B_2 = 10$.

Run no.	K	F	D	$\int \Pi$	$\int U$	$\int D$	K-N_z	z_m
1	5	.20	0	.97	.19	0	.20	42
2	5	.10	0	2.11	.21	0	.21	48
3	5	.01	0	23.96	.24	0	.24	66
4	10	.50	0	.73	.37	0	.37	30
5	10	.20	0	1.99	.39	0	.39	40
6	10	.10	0	4.15	.41	0	.41	48
7	10	.10	.10	4.12	.43	.03	.40	44
8	10	.10	.05	4.13	.42	.02	.40	46
9	10	.10	.01	4.15	.41	0	.41	46
10	10	.01	0	46.17	.47	0	.47	64
11	10	.01	.10	40.30	.86	.53	.36	54
12	20	.20	0	3.95	.79	0	.79	40
13	20	.10	0	8.21	.82	0	.82	46
14	20	.10	.10	8.29	.90	.13	.78	44
15	20	.01	0	90.50	.90	0	.90	62
16	80	.10	0	34.30	3.19	0	3.20	42
17	80	.05	.10	57.90	5.29	2.64	2.96	38
18	100	.05	.10	74.65	6.81	3.49	3.90	36
19	100	.10	0	42.64	3.96	0	3.95	40
20	100	.10	.10	39.30	5.22	1.67	3.65	34
21	100	.20	.10	20.40	4.48	.72	3.65	32

Part B. Effects of changes in the maximal growth rate (μ_m), the extinction of light (L), and the photosynthetic response coefficient (M).

$K = 10$, $S = .1$, $N_0 = 6.3$, $B_1 = 10$, and $B_2 = 10$.

Run no.	μ_m	L	M	F	D	$\int \Pi$	$\int U$	$\int D$	K-N_z	z_m
22	1.5	.06	50	.10	.10	5.7	.59	.03	.58	94
23	1.5	.06	50	.01	.01	68.54	1.00	.30	.77	118
24	1.5	.08	50	.10	.10	4.7	.49	.03	.48	68
25	1.5	.16	50	.10	0	3.71	.37	0	.37	30
26	1.5	.11	75	.10	.10	4.16	.44	.03	.41	50
27	1.5	.11	10	.10	.10	4.04	.40	.03	.37	32
28	1.0	.11	50	.10	.10	4.06	.41	.03	.39	42
29	2.0	.11	50	.10	.10	4.23	.44	.03	.41	48
7†	1.5	.11	50	.10	.10	4.12	.43	.03	.40	44

†This run is listed in part A but is included here for comparison.

Table 2. (Continued)

Part C. The effects of changes in the value of N at $z = 200$ (N_0).

$K = 10$, $F = .1$, $\mu_m = 1.5$, $L = .11$, $M = 50$, $S = .1$, $B_1 = 10$, and $B_2 = 10$.

Run no.	N_0	$\int \Pi$	$\int U$	$\int D$	$K\text{-}N_z$	z_m
7†	6.3	4.12	.43	.03	.40	44
30	31.6	22.25	2.19	0	2.15	48
31	63.2	46.19	4.54	0	4.32	50

Part D. The effects of changes in the half saturation constant for uptake (S).

$K = 10$, $F = .1$, $\mu_m = 1.5$, $L = .11$, $M = 50$, $N_0 = 6.3$, $B_1 = 10$, and $B_2 = 10$.

Run no.	S	$\int \Pi$	$\int U$	$\int D$	$K\text{-}N_z$	z_m
32	1.00	4.10	.41	.01	.37	36
33	.50	4.09	.41	.01	.38	40
7†	.10	4.12	.43	.03	.40	44
34	.01	4.17	.45	.04	.41	50

†This run is listed in part A but is included here for comparison.

in the same region as the maximum in Π. When D is nonzero (Run 7), δ_2 increases below the maximum in Π in effect forming a minimum in δ_2. Otherwise, the profiles for $D = 0$ and $D = 0.1$ are indistinguishable. We will return to a discussion of the model results with respect to field data at the end of this section.

Profiles for the other nitrogen flux terms found in Eqs. 1 and 2 exhibited maxima in their magnitude in the same region as the maximum in Π (Fig. 3c). The profile for the turbulent flux of N, $K \cdot N_{zz}$, is identical to the profile for U. The turbulent flux of Π, $K \cdot \Pi_{zz}$, is negative within the region of the Π maximum and positive outside indicating that Π produced in this region is being transported above and below. The large particle flux term, $F \cdot \Pi$, is of course proportional to the profile for Π.

On the basis of the general results, there appear to be three distinct regions of the model solution. In the upper region, U approaches zero due to very low values for N. With regard to Eq. 3, $N \ll S$ but V_m approaches μ_m due to sufficient light penetration at shallow depths. In the middle region of the model, U is significantly nonzero due to the presence of both sufficient light and NO_3^-. Of course, if Π were zero, U would also be zero. As long as the initial conditions for the model include finite levels of Π, a maximum in Π will form in the region of the maximum in U, contributing to the sharpness of the peak in U. In effect, this middle region of the model represents a zone of balance between the factors which determine U. In the lower region of the model, $N > S$, but light has attenuated such that V_m is near zero. In general, N is turbulently mixed into the well lit region of the model where it is utilized. The vertical position of

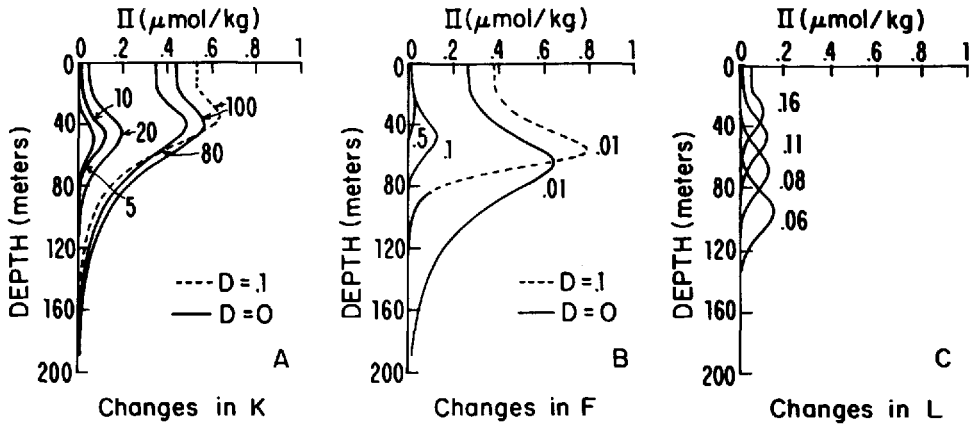

Figure 4. Changes in the profile for Π caused by changing: (A) the vertical eddy diffusivity; K, (B) the particle flux constant; F, and (C) the light extinction coefficient; L.

the maximum in U and Π (z_m) will be determined by the parameters determining the penetration of light downward and the rate of N mixing upward.

With respect to δ_1, isotopic fractionation by N uptake in the middle region of the model results in an increase in δ_1 as N diminishes toward the surface. Note that δ_2 is always less than δ_1 in the middle and upper regions of the model due to isotopic fractionation caused by N uptake. When the decay parameter, D, is nonzero, isotopic fractionation in this process results in an increase in δ_2 in the lower region of the model as Π diminishes with depth. Keeping all other parameters constant, increases in the fractionation factors B_1 and B_2 will increase the amplitude of the vertical variation in these profiles.

4. Results of sensitivity studies

a. Sensitivity of general results to parameter changes. The profile for Π is modified by changes in the parameters K, F, and L (Fig. 4). Increasing turbulent mixing (K) or the residence time for Π (decreasing F), results in the magnification and broadening of the Π maximum. Decreasing the attenuation of light, L, primarily results in the deepening of the Π maximum. In Figures 4a and 4b, the effect of the decay term becomes more significant at high K and low F resulting in modifications in the shape and position of the Π maximum. The factors controlling the significance of the decay term will be discussed in further detail below. Figure 5 illustrates the sensitivity of δ_2 to changes in K, F, and L. Increasing K or decreasing F, reduces the amplitude of the minimum in δ_2 with respect to surface values. Decreasing L lowers the position and increases the amplitude of the minimum in δ_2.

By increasing K and reducing M, it is possible to force the maxima in U and Π to the surface (Fig. 6a). There is only a slight minimum in δ_2 (Fig. 6b) and N has a small but

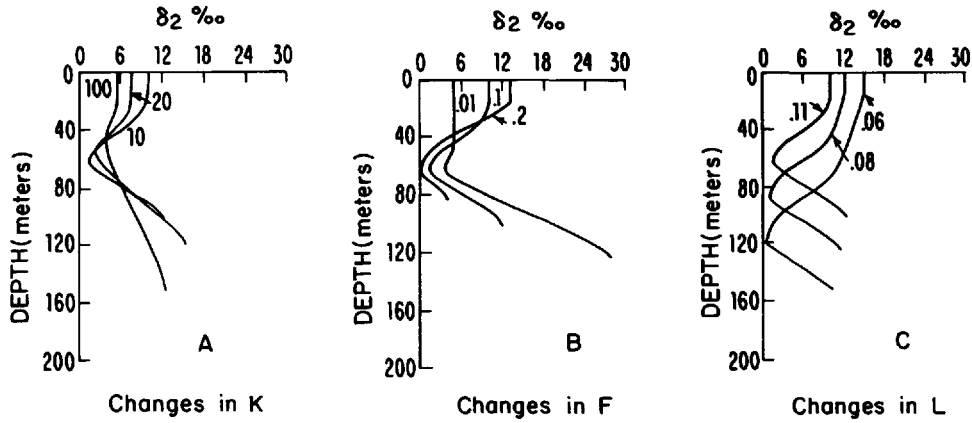

Figure 5. Changes in the profile for δ_2 caused by changing: (A) the vertical eddy diffusivity; K, (B) the particle flux constant; F, and (C) the light extinction coefficient L.

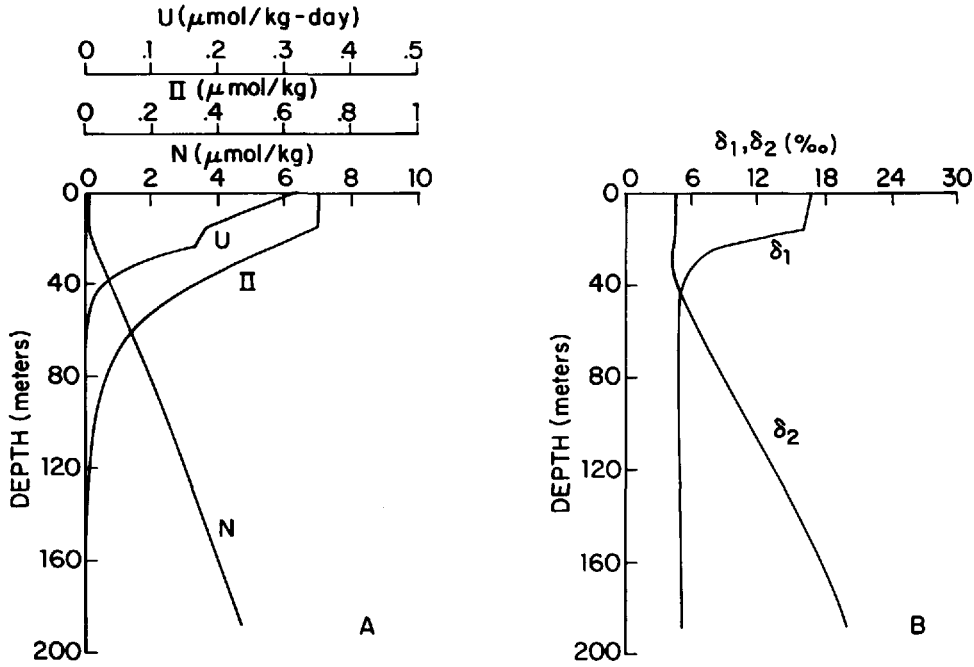

Figure 6. Model solution at a high value for the eddy diffusivity (K = 100) and at a low value for the photosynthetic response coefficient (M = 5). (A) profiles for N, Π, and U. (B) profiles for δ_1 and δ_2.

significant value at $z = 0$ when compared to the value of S; 0.1. This solution for the model may be considered more typical of winter-time, destratified conditions.

b. Sensitivity of integrated quantities. Several features of the model solution can be identified and analyzed for parameter sensitivity. Three important quantities integrated from 0 to 200 m are integrated Π ($\int \Pi$), integrated U ($\int U$), and integrated decay ($\int D$). To integrate the flux of large particles, $F \cdot \Pi$, the value of $F \cdot \int \Pi$ may be simply calculated. Another feature that will be considered is the depth level of the maximum in U and Π (z_m). Table 2 lists for each model run the value for each of these quantities.

At steady state, $\int U - \int D$ should balance the upward turbulent transport of N through the lower boundary of the model. This transport is equivalent to $K \cdot N_z$, where the value of N_z is calculated in the lower region of the model where N_{zz} is zero:

$$\int U = K \cdot N_z + \int D.$$

It appears that an increase in K or a decrease in F will increase the importance of $\int D$ relative to $\int U$ (Table 2, Part A) when D is nonzero. In both cases, a greater amount of Π mixes below the euphotic depth, z_e, either by an increase in turbulent mixing or by an increase in the residence time of Π.

$\int \Pi$ may be related to $\int U$ and $\int D$ by rearrangement of Eq. 2 and integrating both sides with respect to z (assuming the integrated turbulent flux of Π is zero and steady state conditions):

$$\int \Pi = \left(\int U - \int D \right) / F .$$

Assuming that $\int D$ is small compared to $\int U$ the following expression may be derived:

$$\int \Pi = K \cdot N_z / F .$$

This expression is equivalent to the equation presented by Eppley *et al.* (1983) where $1/F$ is the residence time for Π. Figure 7a shows the relationship between $\int \Pi$ and $K \cdot N_z$ for several values of F.

c. Sensitivity of z_m. Changes in K and F also affect the value of z_m (Fig. 7b). The affect of F is much larger and may be related to the increase in Π that accompanies a decrease in F. Due to the dependency of U on Π in Eq. 3, an increase in $\int \Pi$ tends to increase $\int U$. In order that a steady state may be attained, an increase in $K \cdot N_z$ is necessary. This is accomplished by an increase in N_z brought about by an increase in z_m since N_0 is kept constant. Similarly, an increase in N_0 results not only in a near proportional increase in $\int \Pi$ and $\int U$ but also causes an increase in z_m (Table 2, Part C).

The depth of maximal uptake (z_m) is most sensitive to L, M, and μ_m (Table 2, Part

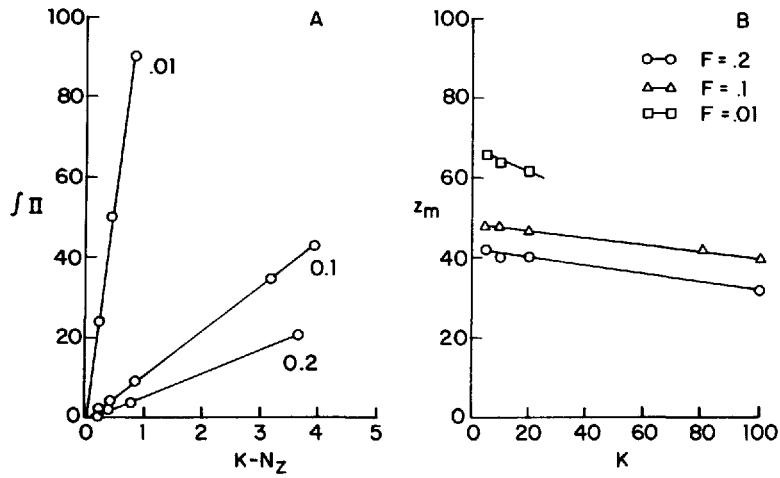

Figure 7. (A) Integrated Π($\int$ Π) vs. $K \cdot N_z$ at several values for F. (B) The depth of the maximum in U, (z_m), vs. K for several values of F.

B). This sensitivity results principally from the dependence of V_m upon these parameters. Figure 8 illustrates the changes in the vertical profile of V_m that occur by changing M, L, or μ_m. L and M both affect the vertical position of the profile with greater sensitivity to changes in L. μ_m affects the amplitude of the profile for V_m. The relative influence upon z_m in order of descending sensitivity is L, M, and μ_m (Table 2, Part B). The sensitivity of the other quantities to these parameters appears to result from their modification of z_m and subsequent changes in N_z.

The half-saturation constant for uptake, S, also affects z_m (Table 2, Part D).

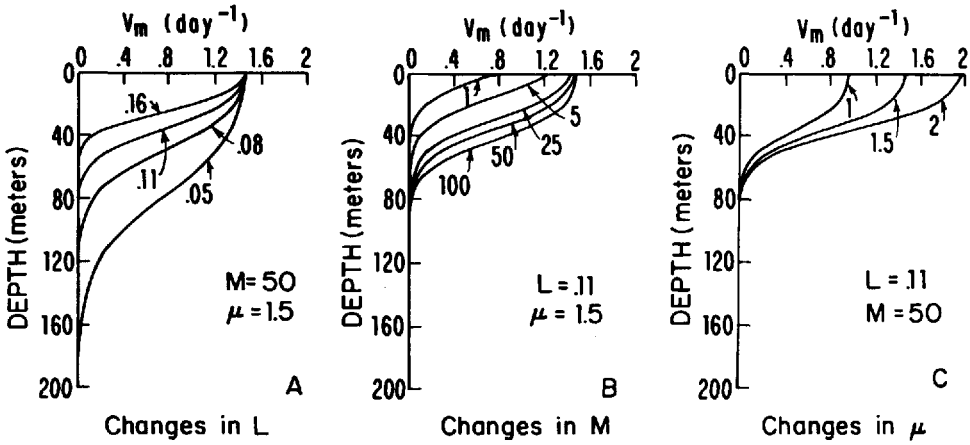

Figure 8. Changes in the profile for V_m with changes in: (A) the light extinction coefficient; L, (B) the photosynthetic response coefficient; M, and (C) the light dependent maximal growth rate; μ_m.

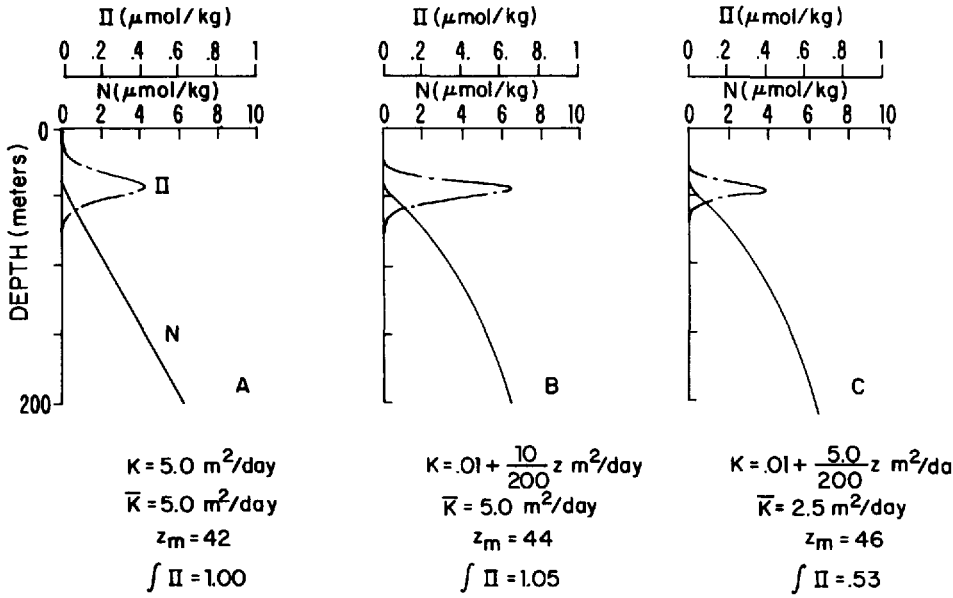

Figure 9. Sensitivity to linearly varying K. N and Π profiles for parameters as in run 1 (Table 2) except K varies linearly. (A) $K = 5$ m^2/day, $\bar{K} = 5$ m^2/day (run 1), (B) $K = .01 + 10/200\ z$ m^2/day, $\bar{K} = 5$ m^2/day, (C) $K = .015/200\ z$ m^2/day, $\bar{K} = 2.5$ m^2/day.

Increasing S, results in a decrease in z_m without altering $\int \Pi$ other than by its affect on N_z. Larger values of S decrease U, forcing the balance between the turbulent flux of N and the downward penetration of light to occur at a shallower depth level.

d. Effects of variable K. The assumption of a constant K is appropriate if it does not significantly affect the results of the sensitivity analysis and the observations of model behavior. To determine an appropriate realistic $K(z)$, the Ring 82-E data were examined. By assuming $T_t = (KT_z)_z \equiv 0$, a $K(z)$, linear in z, was found to be sufficient as it substantially recreated the T profile.

Figure 9 presents a set of profiles from runs with all parameters other than K unchanged. The qualitative behavior is quite similar, however it appears that the value of K near z_m is controlling the width of the Π peak while that near the bottom is controlling the amplitude. Also, the z_m and $\int \Pi$ values vary as expected from the sensitivity analysis. z_m is being controlled by K in the upper portion of the profile while $\int \Pi$ is related to K beneath the euphotic zone. These variations and all of the variable K runs performed were consistent with the constant K sensitivity analysis and general observations of model behavior.

e. Comparison between the model results and field observations. In addition to the qualitative nature of the model solution, it is worthwhile to compare the solution with

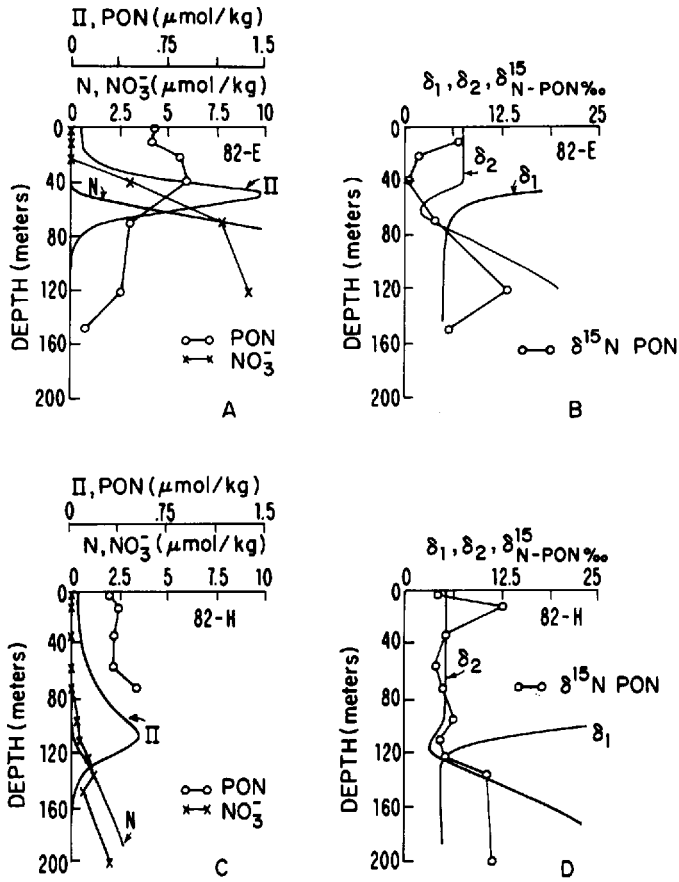

Figure 10. Comparison between model results and field data. (A) Profiles for modelled N, measured NO_3^-, modelled II, and measured PON for Ring 82-E. (B) Profiles for modelled δ_1, δ_2, and the measured $\delta^{15}N$ of PON for Ring 82-E. (C) Profiles for modelled N, measured NO_3^-, modelled II, and measured PON for Ring 82-H. (D) Profiles for modelled δ_1, δ_2, and the measured $\delta^{15}N$ of PON for Ring 82-H.

field data on a more quantitative basis as an evaluation of the limitations of the model. Figure 10 presents the results of two model runs using parameter sets which are most representative of water column conditions for Rings 82-H and 82-E at the time they were sampled. Data from two representative stations are also presented for comparison to model results. The value of L used is 0.11 and 0.06, respectively, based on field measurements of light attenuation with depth (C. Ventsch, pers. comm.). The values of N_0 are 3.15 and 63, respectively. These values for N_0 result in the model reproducing the observed values for N_z at the top of the nitracline which considering the sampling resolution may be considered to be minimal values. The observed $NO_3^-(N)$ profiles were not linear with depth such that the measured NO_3^- concentrations were considerably smaller at 200 m than the value of N_0 used. It is the value of N_z at the top

Table 3. Comparison between model results and field observations.

	Ring 82-E		Ring 82-H	
	Model	Observations	Model	Observations
Integrated PON (μmol)	41	30.5	25	24†
Range in δ_2	5.3	6.7	2.0	8.5
Average δ_2	4.8	3.4	4.6	6.3
Minimum δ_2	2.0	0.0	3.2	4.0
z_{min}(meters)	62	40	116	111
Model Parameters				
K	10		10	
F	0.1		0.01	
D	0.1		0.1	
L	0.11		0.06	
M	50		50	
μ_m	1.5		1.5	
N_0	63		3.15	
B_1	10		10	
B_2	10		10	

†Integrated to 75 m, no data for PON concentration below this depth.

of the nitracline, however, which strongly influences the values of $\int U$ and $\int \Pi$. It is apparent that the model results and the field observations are in good agreement in this respect. The realistic simulation of the lower portion of the NO_3^- profiles probably requires consideration of vertical advection and a vertically varying value for K. The same value of K was used in both runs (10 m^2/day) and was justified by the observation of similar values for stability (E) at the top of the nitracline (data provided by T. Joyce) for both stations in Rings 82-E and 82-H. This value for K was calculated using the equation empirically derived by King and Devol (1979) based on measurements of NO_3^- flux, the vertical NO_3^- gradient, and water column stability:

$$K = 643 \cdot (E \cdot 10^6)^{-1.61}$$

where

$$E = \sigma_{t_z} \cdot 10^{-3}.$$

Values for K in the depth interval corresponding to the top of the nitracline were between 8 and 12 m^2/day.

The values for F used were 0.1 and 0.01, respectively, corresponding to estimates of residence time based on measured values for NO_3^- uptake (J. J. McCarthy, unpublished data). A full listing of the values for the parameters used, a summary of the model results, and the corresponding measured values for Rings 82-E and 82-H are given in Table 3. Note that for the purposes of these comparisons, Π is equated with PON. The average δ_2 values are calculated as weighted average based on PON

concentration. Both average δ_2 and integrated PON values ($\int \Pi$) are calculated only for the depth interval between the surface and the depth of the minimum in $\delta^{15}N$. The range in δ_2 is calculated as the difference between the minimum value and maximum value in the euphotic zone. For the most part, these results of the model are in good agreement with the measured values. For Ring 82-H, integrated PON is calculated only down to 75 m and represents an underestimate. Measurements for PON concentration were not made below 75 m for this station.

For Ring 82-E, however, the model results show a greater depth for the δ_2 minimum and a larger value for integrated PON. Both discrepancies could be accounted for if the residence time ($1/F$) for PON was smaller than the value used. The discrepancies in the average δ_2 and minimum δ_2 values could be accounted for if $\delta_1(N_0)$ was lower by 2.0‰. Similarly, a larger $\delta_1(N_0)$ could account for the differences between the model results and the measured values for δ_2 for Ring 82-H. Alterations in other parameters (see above) could also bring the model and field observation observations into closer agreement with regard to δ_2 values. For Ring 82-H, the principal discrepancy between the modelled and observed profiles for δ_2 is the presence of a near-surface maximum in the observed profile for δ_2. Altabet and McCarthy (1986) concluded that such near-surface maximums must be due to processes other than those which have been included in the model.

Experiments involving variable K were also compared to the data. K was based upon the temperature profile, assuming that $(K \cdot T_z)_z = T_t \sim 0$ (steady state), that the magnitude of K is 0(8.6 m^2/day) at the top of the main thermocline, and that K is linear with depth. The results are quite similar to the constant K case except that the N profile beneath the euphotic zone compares more favorably with the real data.

A significant difference between both model runs and the field observations is the sharpness of the peak in Π. Both model runs demonstrate low values for Π near surface and below the peak in Π. In the oligotrophic ocean, phytoplankton nitrogen accounts for only a small proportion of the suspended PON and instead is primarily composed of detritus (Holligan *et al.*, 1984). The presence of a background of highly refractory detrital PON of long residence time could account for the discrepancy, especially in the lower region of the model. The agreement between the observed values for integrated PON and modelled $\int \Pi$ probably results from the use of observed values of residence time. These values of residence time represent an average of the residence times for phytoplankton, detrital, and other pools of particulate nitrogen.

In both model runs, the average δ_2 is very close to the value of $\delta_1(N_0)$. This is in agreement with the conclusion of Altabet and McCarthy (1985) that the average $\delta^{15}N$ for euphotic zone PON should be similar to the $\delta^{15}N$ of NO_3^- entering the euphotic zone.

5. Discussion and conclusions

The general features of the model solution agree with the data presented in Altabet and McCarthy (1986). The observed occurrence of the top of the nitracline with a

PON maximum and a minimum in the $\delta^{15}N$ of PON concur with the model results. In addition, the depth interval of the modelled maximum in Π corresponds to maximums in the magnitude of the flux terms in Eq. 2 (Fig. 3c). This result agrees with the results of Jamart *et al.* (1977). The successful simulation of the observed vertical pattern for the $\delta^{15}N$ of PON lends additional credence to the general validity of the model.

The discrepancies that do exist between the model results and field observations suggest additional factors which need to be included in future models. The largest discrepancies between the model results and the field observations stem from both the assumption of a constant K and not distinguishing between phytoplankton and detrital nitrogen. The latter not only influences the vertical distribution of Π but also the major flux terms which depend on Π. Vertical variations in K would not only influence the distributions of N and Π due to its effect on mixing but would also affect the vertical transport rates for N.

Next in importance are the assumptions of steady state and one-dimensionality. It appears that, once detached from the Gulf Stream, warm-core rings undergo a series of changes brought about by interaction by surrounding waters and by local meteorology (see Altabet and McCarthy, 1985 and Joyce *et al.*, 1984 as examples). Our recent attachment (Walstad, 1984) of a physical upper-mixed layer model to our eddy resolving open ocean model which assimilates real data (Robinson *et al.*, 1984) provides an opportune context for the development of a more realistic biological model of this type. Examination of a more stable field site may also be appropriate.

More minor contributors to the discrepancy between model and field results include the values used for the various parameters. More accurate estimates for K would be useful and could be derived from dissipation measurements. Field measurements for the $\delta^{15}N$ of NO_3^- would provide an exact value for $\delta_1(N_0)$.

To summarize, the general validity of the model supports the usefulness of this approach for studying the vertical fluxes of nitrogen in the upper-ocean. Discrepancies between the model results and field observations point the way to both future modelling efforts and field studies. The robustness of model results indicates credible key attributes of the natural system, primarily the importance of the balance between the vertical turbulent transport of NO_3^- and the light dependent uptake of NO_3^- by phytoplankton. Significantly, modelling the vertical profiles for the distributions of the $\delta^{15}N$ of NO_3^- and the $\delta^{15}N$ of PON provides a powerful tool for determining the validity of models of this type and for testing hypotheses concerning the factors which determine ^{15}N natural abundance.

Acknowledgments. We thank Professor James J. McCarthy for important contributions to the formulation of the model. Mr. Luke Chung provided helpful analyses of model solutions. This research was supported by NSF grants OCE 80-22990 and OCE-83-14013, and in part by The Education Office of the Woods Hole Oceanographic Institution (MAA).

REFERENCES

Altabet, M. A. and J. J. McCarthy. 1985. Temporal and spatial variations in the natural abundance of ^{15}N in PON from a warm-core ring. Deep-Sea Res., *32,* 755–772.

—— 1986. Vertical patterns in ^{15}N natural abundance in PON from the surface waters of warm-core rings. J. Mar. Res., *44,* 185–201.

Anderson, G. C. 1969. Sursurface chlorophyll maximum in the northeast Pacific Ocean. Limnol. Oceanogr., *14,* 386–391.

—— 1978. Deep ocean mining and the ecology of the tropical North Pacific. Dept. of Oceanography, University of Washington Special Report, *83,* 1–123.

Betzer, P. R., W. J. Showers, E. A. Laws, C. D. Win, G. R. DiTullio and P. M. Kroopnick. 1984. Primary productivity and particle fluxes on a transect of the equator at 153W in the Pacific Ocean. Deep-Sea Res. *31,* 1–11.

Bishop, J. K. B., J. M. Edmond, D. R. Ketten, M. P. Bacon and W. G. Silker. 1977. The chemistry, biology, and vertical flux of particulate matter from the upper 400 meters of the equatorial Atlantic Ocean. Deep-Sea Res., *24,* 511–548.

Bishop, J. K. B. and J. Marra. 1984. Variations in primary production and the particulate carbon flux through the base of the euphotic zone at the site of the Sediment Trap Intercomparison Experiment (Panama Basin). J. Mar. Res., *42,* 189–206.

Cline, J. D. and I. R. Kaplan. 1975. Isotopic fractionation of dissolved nitrate during denitrification in the Eastern Tropical North Pacific Ocean. Mar. Chem., *3,* 271–299.

Cullen, J. J. and R. W. Eppley. 1981. Chlorophyll maximum layers of the Southern California Bight and possible mechanisms of their formation and maintenance. Oceanologica Acta, *14,* 23–32.

Deuser, W. and E. Ross. 1980. Seasonal change in the flux of organic carbon to the deep Sargasso Sea. Nature, *283,* 364–365.

Eppley, R. W. 1972. Temperature and phytoplankton growth in the sea. Fish. Bull., *70,* 1063–1085.

Eppley, R. W. and B. J. Peterson. 1979. Particulate organic matter flux and planktonic new production in the deep ocean. Nature, *282,* 677–680.

Eppley, R. W., E. H. Renger and P. R. Betzer. 1983. The residence time of particulate organic carbon in the surface layer of the ocean. Deep-Sea Res., *30,* 311–323.

Eppley, R. W., E. H. Renger and W. G. Harrison. 1979. Nitrate and phytoplankton production in southern California coastal waters. Limnol. Oceanogr., *24,* 483–493.

Eppley, R. W., J. N. Rogers and J. J. McCarthy. 1969. Half-saturation constants for the uptake of nitrate and ammonia by marine phytoplankton. Limnol. Oceanogr., *14,* 912–920.

Gardner, W. D., K. R. Hinga and J. Marra. 1983. Observations on the degradation of biogenic material in the deep ocean with implications on the accuracy of sediment trap fluxes. J. Mar. Res., *41,* 195–214.

Hoering, T. C. and H. T. Ford. 1960. The isotope effect in the fixation of nitrogen by *Azotobacter.* J. Amer. Chem. Soc., *82,* 376–378.

Holligan, P. M., R. P. Harris, R. C. Newell, D. S. Harbour, R. N. Head, E. A. S. Linley, M. I. Lucas, P. R. G. Tranter and C. M. Weekly. 1984. Vertical distribution and partitioning of organic carbon in mixed, frontal, and stratified waters of the English Channel. Mar. Ecol. Prog. Ser., *14,* 111–127.

Honjo, S. and M. R. Roman. 1978. Marine copepod fecal pellets: production, preservation, and sedimentation. J. Mar. Res., *36,* 45–57.

Jamart, B. M., D. F. Winter, K. Banse, G. C. Anderson and R. K. Lam. 1977. A theoretical study of phytoplankton growth and nutrient distribution in the Pacific Ocean off the northwestern U.S. coast. Deep-Sea Res., *24,* 753–773.

Joyce, T., R. Backus, K. Baker, P. Blackwelder, O. Brown, T. Cowles, R. Evans, G. Fryxell, D. Mountain, D. Olson, R. Schlitz, R. Schmitt, P. Smith, R. Smith and P. Wiebe. 1984. Rapid evolution of a Gulf Stream warm-core ring. Nature, *308,* 837–840.

Kiefer, D. A. and J. N. Kremer. 1981. Origins of vertical patterns of phytoplankton and nutrients in the temperate open ocean: a stratigraphic hypothesis. Deep-Sea Res., *28,* 1087–1105.

King, F. D. and A. H. Devol. 1979. Estimates of vertical eddy diffusion through the thermocline from phytoplankton nitrate uptake rates in the mixed layer of the Eastern Tropical Pacific. Limnol. Oceanogr., *24,* 645–651.

Liu, K. 1979. Geochemistry of nitrogen compounds in two marine environments: the Santa Barbara Basin and the ocean off Peru. Doctoral thesis, University of California, Los Angeles, CA, 354 pp.

Lorenzen, C. J. and N. A. Welschmeyer. 1983. The *in situ* sinking rates of herbivore fecal pellets. J. Plank. Res., *8,* 929–933.

Mariotti, A. 1983. Atmospheric nitrogen is a reliable standard for natural $\delta^{15}N$ abundance measurements. Nature, *303,* 685–687.

Miyake, Y. and E. Wada. 1967. The abundance ratio of $^{15}N/^{14}N$ in marine environments. Rec. Oceanogr. Works Japan, *9,* 37–53.

Robinson, A. R., J. A. Carton, C. N. K. Mooers, L. J. Walstad, E. F. Carter, M. M. Rienecker, J. A. Smith and W. G. Leslie. 1984. A real-time dynamical forecast of ocean synoptic/mesoscale eddies. Nature, *309,* 781–783.

Shanks, A. L. and J. D. Trent. 1979. Marine snow: Microscale nutrient patches. Limnol. Oceanogr., *24,* 850–854.

Suess, E. 1980. Particulate organic carbon flux in the oceans: surface productivity and oxygen utilization. Nature, *288,* 260–263.

Venrick, E. L., J. A. McGowen and A. W. Mantyla. 1973. Deep maxima of photosynthetic chlorophyll in the Pacific Ocean. Fish. Bull., *71,* 41–52.

Wada, E. and A. Hattori. 1978. Nitrogen isotope effects in the assimilation of inorganic nitrogenous compounds by marine diatoms. Geomicrobiol. J., *1,* 85–101.

Walstad, L. J. 1984. Upper layer model and assimilation of satellite IR imagery. EOS, *65,* 939 (abstract).

Received: *5 December, 1984;* revised: *18 September, 1985.*